Electrochimica Acta 162 (2015) 224–229

Contents lists available at ScienceDirect

Electrochimica Acta

journal homepage: www.elsevier.com/locate/electacta

Iron-tetracyanobenzene complex derived non-precious catalyst for oxygen reduction reaction

Ja-Yeon Choi [a], Drew Higgins [a], Gaopeng Jiang [a], Ryan Hsu [a], Jinli Qiao [b,**], Zhongwei Chen [a,*]

[a] Department of Chemical Engineering, Waterloo Institute for Nanotechnology, University of Waterloo, Waterloo, Ontario N2L 3G1, Canada
[b] College of Environmental Science and Engineering, Donghua University, 2999 Ren'min North Road, Shanghai 201620, PR China

ARTICLE INFO

Article history:
Received 28 May 2014
Received in revised form 17 November 2014
Accepted 18 November 2014
Available online 20 November 2014

Keywords:
Fuel cells
Oxygen reduction
Non-precious metal catalyst
Electrocatalysis

ABSTRACT

Non-precious metal oxygen reduction reaction (ORR) catalysts were prepared by pyrolyzing a carbon supported complex consisting of iron acetate coordinated with 1,2,4,5-tetracyanobenzene (TCNB) in an iron phtalocyanine-like polymer arrangement. The effect of heat treatment temperature is systematically investigated from 700 to 1000 °C, with ORR activity investigated by half-cell electrochemical evaluation in 0.1 M $HClO_4$. The highest ORR performance is obtained for the sample heat treated at 1000 °C, with this sample demonstrating high (>98%) selectivity towards the efficient 4 electron reduction mechanism, comparable with some of the best non-precious metal catalysts reported to date. The physical and surface properties of the prepared catalysts were investigated by high-resolution transmission electron microscopy (TEM), fourier transform infrared (FTIR) spectroscopy, X-ray diffraction (XRD), X-ray photoelectron spectroscopy (XPS), thermogravimetric analysis (TGA) and BET surface area analysis. After heat treatment, a thin (<10 nm) coating was observed on the surface of the carbon supports, attributed to residual species remaining from the heat treated precursor complex that provide the source of ORR activity.

1. Introduction

The development of efficient oxygen reduction reaction (ORR) catalysts is essential for the widespread commercialization of polymer electrolyte fuel cells (PEFCs) due to the importance of the reaction kinetics in controlling device performance [1–3]. Platinum and platinum-alloy based catalysts are conventionally used owing to their high intrinsic ORR activity and stability; however the high cost and monopolized global distribution hinders the long term economic feasibility of PEFC systems. This has inspired significant research efforts to the development of low cost, non-precious metal based catalysts to replace platinum-based materials.

Since the initial discovery in 1964 by Jasinski *et al.* [4] that demonstrated cobalt phtalocyanine (CoPc) materials were active for the ORR, significant progress has been made towards the development of transition metal (M=Fe or Co)-nitrogen-carbon complexes, commonly referred to as M—N—C systems. Early investigations illustrated the importance of heat treating transition metal macrocycles at temperatures up to 1000 °C to realize significant performance and stability gains [5–7]. Years later the discovery was made that pyrolyzing a mixture of relatively inexpensive transition metal, nitrogen and carbon precursor materials could produce highly active M—N—C catalyst materials [8,9]. Owing to the heterogeneous complexity of the resulting catalyst structures, there still remains debate in the literature over the exact identity and nature of the catalytically active sites, with contrasting opinions over whether the transition metal species comprises the active site, or merely plays an integral role in active site formation [3]. Regardless, it has been well established that the structure, properties and resulting ORR activity of heat treated M—N—C complexes is directly governed by the particular precursor materials employed and synthetic processes utilized [10–16].

While several catalysts have been prepared by pyrolyzing transition metal-phtalocyanine (i.e. FePc, CoPc) macrocycles absorbed on the surface of carbon supports [17–21], the bulky sheet-like structure of these molecules can arise some challenges including poor dispersion on the carbon support and molecular overlap resulting in iron agglomeration during the heat treatment. Alternatively it is possible to prepare FePc polymer sheets *in situ*

* Corresponding author. Tel.: +1 519 888 4567x38664.
** Corresponding author. Tel.: +86 21 67792379.
E-mail addresses: qiaojl@dhu.edu.cn (J. Qiao), zhwchen@uwaterloo.ca (Z. Chen).

http://dx.doi.org/10.1016/j.electacta.2014.11.118
0013-4686/

from relatively inexpensive iron acetate and 1,2,4,5-tetracyanobenzene (TCNB) [22–24]. By employing these small precusursor molecules, it is expected that more uniform and complete coverage of the carbon support material can be obtained, and by using the *in situ* formation and polymerization of FePc, effective iron-center segregation can be achieved. Herein, we heat treat iron acetate and TCNB adsorbed on the surface of Ketjen black carbon supports at 300 °C and then subsequently at 400 °C to promote the formation of polymeric FePc sheets with planar geometry over the carbon support and form strong molecular interactions. After collection, the obtained materials were systematically pyrolyzed at temperatures ranging from 700 to 1000 °C and then were characterized and investigated for ORR activity in an acidic electrolyte to determine synthesis-property-performance relationships for this newly developed non-precious catalyst.

2. Experimental

2.1. Catalyst synthesis

The Ketjenblack EC-600J (AkzoNobel Corporate) carbon black support was first functionalized to increase solvent dispersion and precursor reactions [25] by a procedure described in our previous work [26]. Briefly, 5 g of the carbon black was first dissolved into 6 M HCl for 2 hours at room temperature to remove metal impurities. The sample was air filtered and washed with copious amounts of D.I. water. This treatment was followed by refluxing the carbon black in 70% HNO_3 at 80 °C in air for 8 hours before filtering. The precipitate product was washed with copious amounts of D.I. water and dried at 60 °C overnight to obtain the functionalized Ketjenblack EC-600J (KJ600).

0.0178 g of TCNB (Sigma Aldrich, 97%) and 0.0174 g of iron(II) acetate (FeAc) (Sigma Aldrich, 95%) were dissolved in 10 mL of quinoline for 30 minutes under N_2 protection and at room temperature. 0.3168 g of KJ600 was added to the mixture and stirred for 30 minutes. Still under N_2 protection, the temperature was raised to 210 °C for 24 hours and continuously refluxed. After cooling, 200 mL of methanol was added to precipitate out the solid, which was then filtered, washed with methanol and dried in an overn at 60 °C overnight. The sample was then heat-treated in a reaction furnace at 300 °C for 1 hour, at 400 °C for 1 hour and finally for 1 hour at a final heat-treatment temperature ranging from 700–1000 °C. N_2 was used to flow through the reaction chamber during pyrolysis. The furnace was allowed to cool before the samples were removed and utilized as the final catalyst product. The catalysts are denoted as Fe-TCNB/C-X where X is the final heat-treatment temperature. The catalyst obtained without the final heat-treatment is denoted as Fe-TCNB/C-0.

2.2. Physicochemical characterization

Catalyst samples were analyzed using TEM through a Philips CM300 operating at 300 kV to observe the surface morphology. A Thermal Scientific K-Alpha XPS spectrometer (150 eV) was used to investigate the relative content of different elements on the surface of the synthesized catalysts. Narrow range XPS scans of the N1s peaks were conducted to determine the relative amounts of each nitrogen species present in the catalysts. TGA was conducted using a TGA Q500 to determine the thermal behaviour of the phthalocyanine polymer formed with TCNB and the thermal stability of each of the catalyst samples. Monochromatic CuKα X-rays were used with an Inel XRG 3000 diffractometer to conduct XRD to observe the crystal structures present in the catalysts. A broad range scan of 2θ from 0.288–80.0° was carried out at a rate of 5° min^{-1}. Fourier transform infrared (FTIR) spectra were recorded on a Bruker Tensor 27 FTIR spectrometer in KBr media. The BET surface area and the pore volume of the catalysts were analysed using a Micromeritics ASAP 2020 Surface Area and Porosity Analyzer.

2.3. Electrochemical characterization

Electrocatalytic ORR activity for each synthesized catalyst was evaluated using rotating ring disk electrode (RRDE) voltammetry. The instruments used include a bipotentiostat and a rotation speed controller (Pine Research Instrumentation). The RRDE experiment was carried out in 0.1 M $HClO_4$ electrolyte and using an Ag/AgCl reference electrode. The disk potential was varied from −0.25 to 0.95 V *vs.* Ag/AgCl at a potential sweep rate of 10 mV s^{-1}, and the ring potential was held constant at 1.0 V *vs.* Ag/AgCl. All figures are reported against the reversible hydrogen electrode (V *vs.* RHE).

The catalyst ink deposited on the glassy carbon disk consisted of 4 mg of catalyst suspended in 2 mL of 0.2 wt% Nafion solution. For each RRDE experiment, 40 μL of catalyst ink was deposited onto the glassy carbon electrode with a diameter of 5 mm and allowed to dry. Electrochemical potential sweeps were first conducted with the electrolyte saturated in nitrogen as a background. Bubbling oxygen gas was then used to saturate the electrolyte solution for 30 minutes before potential sweeps were conducted at 1600 rpm to evaluate the ORR activity.

3. Results and discussion

Catalyst morphology and surface structure following synthesis was investigated by TEM with results from Fe-TCNB/C-900 displayed in Fig. 1. For comparison, a TEM image of the carbon support pyrolyzed under the same conditions, albeit in the absence of TCNB precursor materials is given in Fig. 1a. For both the pyrolyzed Ketjenblack and Fe-TCNB/C-900, carbon black supports with particle sizes of ca. 30–50 nm in diameter are clearly observed, while the Fe-TCNB/C-900 catalyst shows a coating layer of less than ca. 10 nm in thickness on the surface. This coating is expected to comprise the residual products remaining after the pyrolysis of the iron and nitrogen precursors that occurs at these elevated temperatures. The coating is relatively uniform over the entire surface of the carbon support

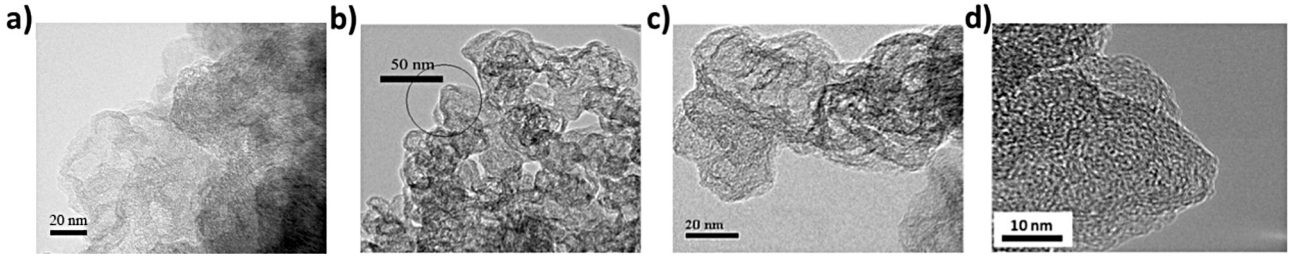

Fig. 1. TEM images of (a) KJ600 pyrolyzed at 900 °C and (b) Fe-TCNB/C-900 with area of (c) high resolution TEM image indicated by the black circle.

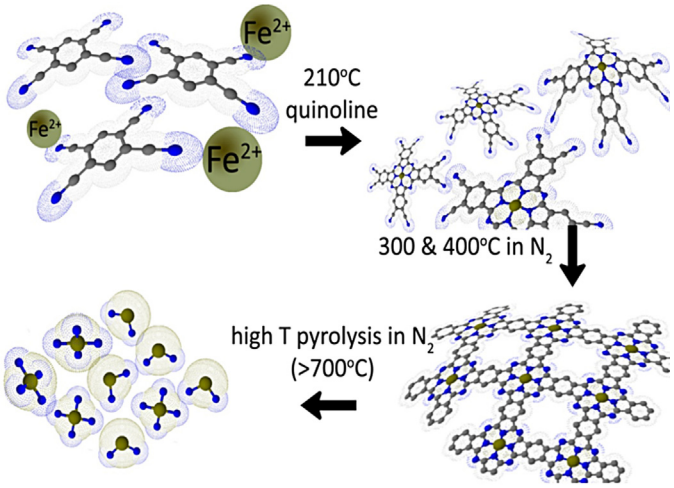

Fig. 2. Proposed structural transformations of precursor molecules on the surface of carbon supports during the various stages of catalyst synthesis.

materials, indicating that the catalyst synthesis technique utilized was effective in terms of good precursor distribution. The speculated structural transformations occurring for the precursor molecules on the surface of the carbon support are provided in Fig. 2. This schematic depicts the main steps that occur during synthesis, including: (1) nitrogen and iron precursors are first dissolved in quinoline at 210 °C to form FePc monomeric units [27]; (2) a heat-treatment at 300 and 400 °C in N_2 cause the monomeric units to polymerize on the surface of the carbon black [22,28]; and (3) the sheet polymers on carbon support enter a high temperature pyrolysis in N_2 which decompose the polymer into the NPMC active sites.

The evidence of metal phthalocyanine structure formation was obtained using FTIR spectroscopy after the 400 °C heat treatment (Fe-TCNB/C-400). The obtained spectrum along with that of KJ600 is provided in Fig. 3. For Fe-TCNB/C-400, the obtained results show a strong resemblance to previously reported metal containing polyphthalocyanines synthesized using TCNB as the monomer [29]. The peak observed at 911 cm^{-1} is known to be associated with metal ligand vibrations and the wavenumber matches closely with that previously reported for FePc [30]. The strongest peak oabtained at 1108 cm^{-1} is attributed to C—H bond in plane bending and Cα—Cβ bond stretching in FePc. In addition, the strong peak observed at 1330 cm^{-1} corresponds to C=C or C=N stretching vibrations in the pyrrole ring in the plane of the FePC macrocycle [31–33]. Another strong peak observed at 1517 cm^{-1} is attributed to the expansion of pyrrole rings as well as $C\alpha—N_c—C\alpha$ and $C—N_m$ stretching [30]. This provides a strong evidence for a successful formation of FePc structure from TCNB monomers on the carbon support.

XRD was utilized to investigate the crystalline structures existent in the catalyst samples, with patterns shown in Fig. 4 for Fe-TCNB/C-800, Fe-TCNB/C-900 and Fe-TCNB/C-1000. The peak at ca. 25° (denoted with ○) in all the samples is attributed to the (0 0 2) plane reflection of graphitic carbon. The diffraction peaks at 44 and 65° correspond to the (1 1 0) plane of α–Fe(denoted with ▲) and the (2 0 0) plane of α–Fe(denoted with ▼), respectively. Fe_3C was also shown to be present in the catalyst structure with characteristic peaks observed at 38, 43 and 78°. The presence of these iron-based crystallites indicate that iron migration and coalescence occurs during the high temperature heat treatment process and is consistent with results of previous reports on M—N—C catalyst development [16,34,35].

Elemental surface concentrations for each prepared catalyst material were quantified by XPS and summarized in Table 1. All samples displayed similar surface iron contents, which is to be expected owing to the identical nominal iron precursor concentrations used for catalyst preparation. Furthermore, the nominal iron content is more than sufficient to generate good ORR activity (ca. > 0.1 wt. %)[36–38], and should not be a governing factor for the catalysts prepared at different temperatures in this work. It is more likely that the content and identity of the nitrogen dopant species influences ORR activity, an observation that has been reported in several different investigations. At increased heat treatment temperatures from 700 to 1000 °C, the nitrogen content was found to decrease from a maximum of 2.79 at. % in Fe-TCNB/C-700, to 1.20 at. % in Fe-TCNB/C-1000. This decrease in nitrogen concentration is a common observation, owing to the instability of some nitrogen species at elevated heat treatment temperatures [39,40].

The high resolution N1s spectra for each sample were deconvoluted into four peaks representing different nitrogen species with results displayed in Fig. 5. The observed peaks can be attributed to pyridinic (398 ↔ 399 eV), pyrrolic (399.9 ↔ 400.5 eV), graphitic (401 ↔ 402 eV), and oxidized (402 ↔ 410 eV) nitrogen species [41–43], with their relative contributions to the N1s peak signal of each sample summarized in Table 2. At increased heat treatment temperatures, the relative contents of both pyridinic and pyrrolic nitrogen species decreases, accompanied by a simultaneous increase in the relative content of graphitic nitrogen. This observation is consistent with results from previous reports,

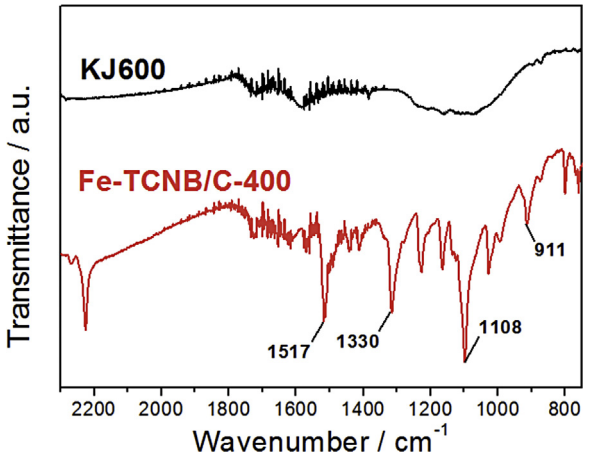

Fig. 3. FTIR spectra of KJ600 and Fe-TCNB/C-400 in KBr pellet.

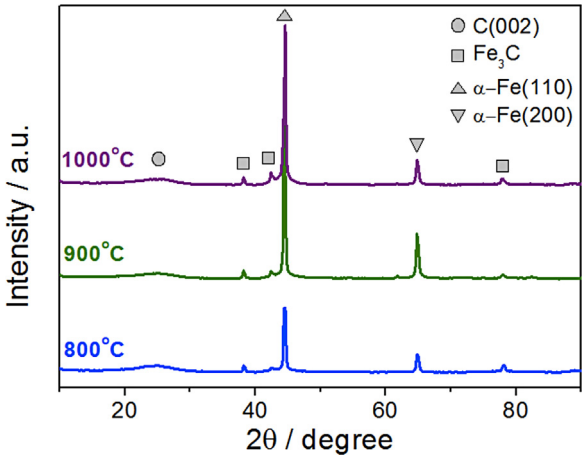

Fig. 4. XRD patterns for catalysts synthesized at 800, 900 and 1000 °C.

Table 1
Surface atomic contents of synthesized catalysts determined by XPS.

Catalyst Sample	C	Fe	N	O
	Atom %			
Fe-TCNB/C-700	94.96	0.06	2.79	2.19
Fe-TCNB/C-800	95.45	0.07	1.94	2.54
Fe-TCNB/C-900	95.18	0.06	1.51	3.25
Fe-TCNB/C-1000	94.70	0.07	1.20	4.03

Table 2
Relative nitrogen species contents determined by XPS N1s peak deconvolution.

Catalyst Sample	Pyridinic	Graphitic	N-oxide	Pyrrolic
	Atom % of nitrogen atoms scanned			
Fe-TCNB/C-700	37.69	38.27	15.21	8.82
Fe-TCNB/C-800	34.09	34.29	17.37	14.25
Fe-TCNB/C-900	26.40	45.63	26.29	1.68
Fe-TCNB/C-1000	24.94	51.60	21.10	2.36

and is owing to the increased stability and favourable formation of graphitic nitrogen [44,45] residing in a six-membered ring formation and residing on the basal plane of graphitic structures.

To determine and verify the thermal behavior of the proposed polyphthalocyanine structure, TGA under nitrogen was carried out on the non-pyrolyzed Fe-TCNB/C mixture and the results are shown in Fig. 6a. Based on the previously reported thermal decomposition behavior of metal phthalocyanine materials, decomposition begins at temperatures above 220 °C, with minor and major decomposition for FePc occuring at 220 and 275 °C, respectively [46,47]. For Fe-TCNB/C, the majority of weight loss occurs from 240 to 260 °C, with some losses as lower and higher temperatures, corresponding well to the reported values. Based on FTIR results and the proposed structural transformations, the metal–nitrogen precursor complexes that did not decompose at temperatures below *ca.* 400 °C underwent physical cross-linking, forming the polymeric phtalocyanine matrix on the surface of carbon. This cross-linking leads to enhanced thermal stability, with decomposition of these species not observed until the temperature reaches 700 °C [47,48]. To evaluate the effect of different pyrolysis temperatures on the as-prepared catalysts, TGA under oxygen was carried out, with curves illustrating the percentage weight remaining versus temperature displayed in Fig. 6b. It can be seen that all TGA curves have a similar shape showing a significant weight loss in the temperature range from 400 to 600 °C. By investigating the derivative weight change plot shown in Fig. 6c, four distinct peaks are clearly observed for Fe-TCNB/C-700. The first peak, located at ca. 409 °C is relatively small and is not observed in the catalyst samples heat-treated at higher temperatures (800 °C or greater). This is expected to arise from species present on the surface of the catalyst that did not decompose at 700 °C. It is expected that the onset of weight loss above 700 °C in N_2 for the non-pyrolyzed Fe-TCNB/C mixture (Fig. 6a) arises from the same species. In this TGA, the additional and significant weight loss observed at temperatures higher than 800 °C can also likely be linked to the weight loss peak for Fe-TCNB/C-700 and Fe-TCNB/C-800 at *ca.* 444 °C in air, arising from complex species formed on the surface of the carbon catalyst during pyrolysis. Beyond that, the majority of weight loss for all the samples was observed at heat treatment temperatures above *ca.* 460 °C. Interestingly the onset of this weight loss is shifted to higher temperatures with the increase of catalyst heat treatment temperature. This indicates that the thermal stability of the catalyst materials are increased under these conditions, most likely arising due to a more graphitic carbon structure formed at higher synthesis temperatures [49].

The ORR activity of the prepared catalysts was evaluated by RRDE in 0.1 M $HClO_4$, with results depicted in Fig. 7a. All ORR

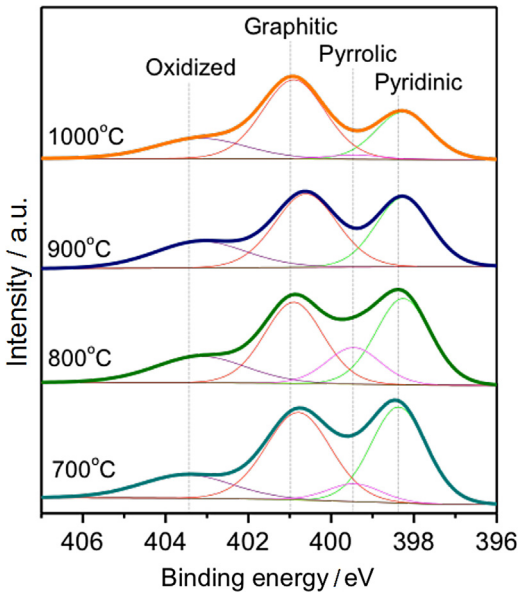

Fig. 5. High resolution XPS N1s scans for catalyst materials prepared at various temperatures.

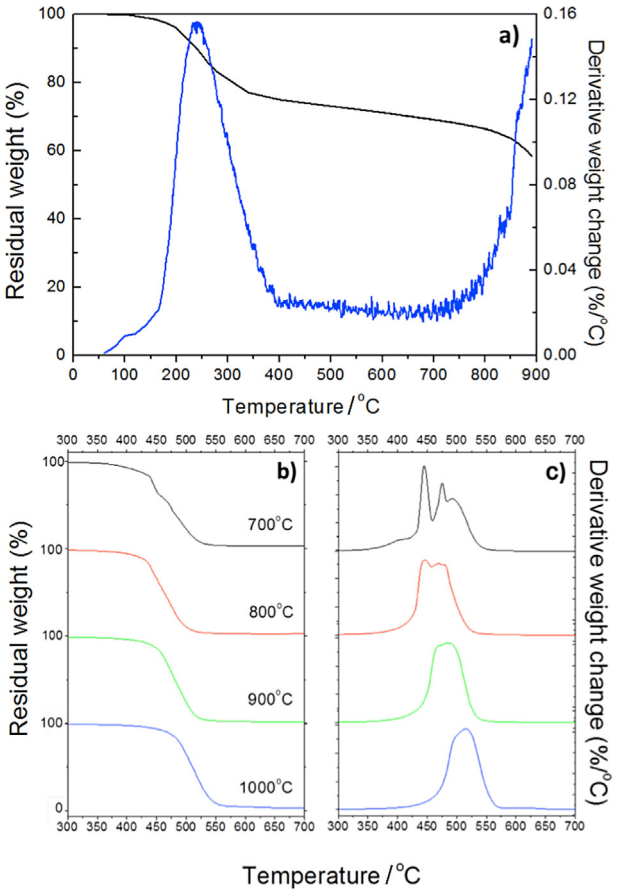

Fig. 6. TGA data obtained (a) under nitrogen environment for non-pyrolyzed Fe-TCNB/C mixture; (b) under oxygen environment for various post pyrolysis samples showing percent weight remaining and (c) derivative weight change versus temperature.

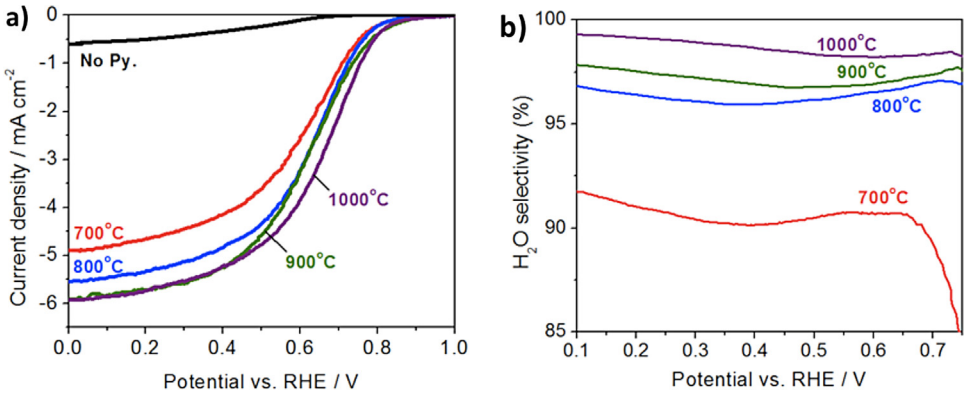

Fig. 7. (a) ORR polarization curves and (b) H_2O selectivities for catalysts prepared at various temperatures obtained at 1600 rpm in O_2 saturated 0.1 M $HClO_4$.

curves present in the figure have been corrected by removing the background signals obtained in N_2 saturated electrolyte. For the sample prepared in the absence of a high temperature pyrolysis, negligible ORR activity is observed, highlighting that the high temperature heat treatment is essential for inducing high catalytic activity. For the catalysts heat-treated at increasing temperatures from 700 to 1000 °C, a clear performance increase is observed in terms of ORR onset potential, mass transport limited current densities and half-wave potentials (Table 3). By processing ring current data, the selectivity of the prepared catalysts towards the overall 4 electron reduction of oxygen was determined and displayed in Fig. 7b. Consistent with the trend observed in terms of ORR activity, increased heat treatment temperatures resulting in higher selectivity towards the 4 electron reduction mechanism. Approximately 98.5% selectivity towards the formation of water is achieved on Fe-TCNB/C-1000 at an electrode potential of 0.4 V *vs.* RHE, a value that is consistent with some of the best non-precious metal catalysts reported to date [11]. The increase in ORR activity observed with increased pyrolysis temperatures can likely be linked to the complete decomposition of the FePc-like structures formed by the processing of iron acetate and TCNB on the surface of the functionalized carbon supports. Interestingly, an increase in ORR activity and selectivity towards the 4 electron ORR mechanism is observed with an increased relative content of graphitic nitrogen present in the materials, although with decreasing overall nitrogen content. While this may indicate that the relative content of graphitic nitrogen species may contribute to enhanced ORR activity, it is likely that a complicated interplay between various nitrogen and/or iron species that results in performance increases. For the present catalyst system, the formation of these species is maximized at 1000 °C based on the observed increases in onset and half-wave potentials. The complicated nature of the active site(s) in these highly heterogeneous non-precious catalysts still remains a contentious issue [8], and thorough fundamental investigations that rely on a wide array of surface and bulk characterization techniques will be required to elucidate their identity.

In order to examine the dependence of the activity on the heat treatment and the induced changes in the physical properties of the materials, the BET surface area and the corresponding pore volume were determined and listed in Table 4. A tremendous decrease in the BET surface area from pristine Ketjen Black ($1440\ m^2\ g^{-1}$) was observed for Fe-TCNB/C-0 (98.7% loss) and Fe-TCNB/C-400 (99.4% loss) owing to the pore closure by the metal-nitrogen precursor complex and the polymeric phthalocyanine matrix, respectively. As the heat treatment temperature increases, decomposition of the phthalocyanine matrix leads to increased surface area and pore volumes, and both values peak at 800 °C due to decomposition of the majority of these surface residing species. Although it is evident that the decomposition of the intermediate species and the arising surface area recovery are essential in achieving catalytic activity, unlike the activity trend, the BET surface area and pore volume values decrease for the samples that undergo pyrolysis at temperatures higher than 800 °C. This implies that the surface area and pore volume are not the only factors affecting the activity of this type of catalysts. The surface area loss observed at temperatures over 800 °C can be attributed to the transformation of amorphous carbon into more ordered graphitic carbon structures [50] as well as agglomeration of carbon nanoparticles into bigger particles at higher temperatures [51]. These temperatures, up to 1000 °C, clearly provide improved ORR activity, with still sufficient enough surface area ($599.5\ m^2\ g^{-1}$) to provide sufficient reactant accessibility to the catalytically active sites. Further studies including a modification of the synthesis conditions to maximize the surface area as well as the nitrogen content at pyrolysis temperatures above 800 °C may lead to improved catalytic activity and better understanding of factors underlying performance.

Table 3
ORR performance parameters for synthesized catalysts.

Catalyst	Current Density at 0.4 V *vs.* RHE ($mA\ cm^{-2}$)	Onset potential (V *vs.* RHE)[a]	Half-wave potential (V *vs.* RHE)	H_2O Selectivity at 0.4 V *vs.* RHE (%)
Fe-TCNB/C-0	0.33	0.60	–	–
Fe-TCNB/C-700	4.15	0.84	0.63	90.2
Fe-TCNB/C-800	4.84	0.84	0.65	96.1
Fe-TCNB/C-900	5.25	0.87	0.66	97.1
Fe-TCNB/C-1000	5.26	0.88	0.68	98.5

[a] Onset potential is defined as the potential at which a current density of 0.1 $mA\ cm^{-2}$ is achieved [11].

Table 4
Surface area and pore volumes determined from BET analysis.

Catalyst	BET Surface Area ($m^2\ g^{-1}$)	Pore Volume ($cm^3\ g^{-1}$)
Fe-TCNB/C-0	19.3	0.02
Fe-TCNB/C-400	8.5	0.04
Fe-TCNB/C-700	501.7	0.98
Fe-TCNB/C-800	726.4	1.62
Fe-TCNB/C-900	671.4	1.39
Fe-TCNB/C-1000	599.5	1.10

4. Conclusions

ORR active non-precious metal catalysts were prepared by heat treating a carbon supported iron-TCNB complex at temperatures ranging from 700 to 1000 °C. The highest ORR activity in 0.1 M $HClO_4$ was observed for Fe-TCNB/C-1000 catalyst, demonstrating an onset potential of ca. 0.88 V *vs.* RHE and a 4 electron reaction selectivity greater than 98% at all electrode potentials investigated, a value comparable with some of the best non-precious metal catalysts reported to date. Based on high-resolution TEM imaging, the observed ORR likely arises from a thin (<10 nm) surface layer formed during the heat treatment of the surface coordinated iron-TCNB complex.

Acknowledgements

This work was supported by the University of Waterloo, the Waterloo Institute for Nanotechnology and the Natural Sciences and Engineering Research Council of Canada (NSERC). This research was also conducted as part of the Catalysis Research for Polymer Electrolyte Fuel Cells (CaRPE FC) Network administered from Simon Fraser University and supported by Automotive Partnership Canada (APC) Grant No. APCPJ 417858-11 through NSERC.

References

[1] Z. Chen, D. Higgins, A. Yu, L. Zhang, J. Zhang, Energy Environ. Sci. 4 (2011) 3167–3192.
[2] F. Jaouen, E. Proietti, M. Lefevre, R. Chenitz, J.-P. Dodelet, G. Wu, H.T. Chung, C.M. Johnston, P. Zelenay, Energy Environ. Sci. 4 (2011) 114–130.
[3] D.C. Higgins, Z. Chen, Canadian J. Chem. Eng. 91 (2013) 1881–1895.
[4] R. Jasinski, Nature 201 (1964) 1212–1213.
[5] R. Franke, D. Ohms, K. Wiesener, J. Electroanal. Chem. Inter. Electrochem. 260 (1989) 63–73.
[6] J.A.R. van Veen, H.A. Colijn, J.F. van Baar, Electrochim. Acta 33 (1988) 801–804.
[7] K. Wiesener, Electrochim. Acta 31 (1986) 1073–1078.
[8] S. Gupta, D. Tryk, I. Bae, W. Aldred, E. Yeager, J. Appl. Electrochem. 19 (1989) 19–27.
[9] D. Ohms, S. Herzog, R. Franke, V. Neumann, K. Wiesener, S. Gamburcev, A. Kaisheva, I. Iliev, J. Power Sources 38 (1992) 327–334.
[10] G. Wu, P. Zelenay, Acc. Chem. Res. 46 (2013) 1878–1889.
[11] G. Wu, K.L. More, C.M. Johnston, P. Zelenay, Science 332 (2011) 443–447.
[12] H.T. Chung, C.M. Johnston, K. Artyushkova, M. Ferrandon, D.J. Myers, P. Zelenay, Electrochem. Commun. 12 (2010) 1792–1795.
[13] E. Proietti, F. Jaouen, M. Lefèvre, N. Larouche, J. Tian, J. Herranz, J.-P. Dodelet, Nat. Commun. 2 (2011) 416.
[14] M. Lefèvre, E. Proietti, F. Jaouen, J.-P. Dodelet, Science 324 (2009) 71–74.
[15] J.-Y. Choi, D. Higgins, Z. Chen, J. Electrochem. Soc. 159 (2011) B86–B89.
[16] J. Wu, W. Li, D. Higgins, Z. Chen, The Journal of Physical Chemistry C 115 (2011) 18856–18862.
[17] M. Ladouceur, G. Lalande, D. Guay, J.P. Dodelet, L. Dignard-Bailey, M.L. Trudeau, R. Schulz, J. Electrochem. Soc. 140 (1993) 1974–1981.
[18] L. Dignard-Bailey, M.L. Trudeau, R.S.A. Joly, G. Lalande, D. Guay, J.P. Dodelet, J. Mater. Res (1994) 3203–3209.
[19] L.T. Weng, P. Bertrand, G. Lalande, D. Guay, J.P. Dodelet, Appl. Surf. Sci 84 (1995) 9–21.
[20] G. Lalande, G. Faubert, R. Cote, D. Guay, J.P. Dodelet, L.T. Weng, P. Bertrand, J. Power Sources 61 (1996) 227–237.
[21] G. Lalande, R. Côté, G. Tamizhmani, D. Guay, J.P. Dodelet, L. Dignard-Bailey, L.T. Weng, P. Bertrand, Electrochim. Acta 40 (1995) 2635–2646.
[22] M. Abel, S. Clair, O. Ourdjini, M. Mossoyan, L. Porte, J. Am. Chem. Soc. 133 (2010) 1203–1205.
[23] W. He, M. Lieberman, J. Porphyrins Phthalocyanines 15 (2011) 277–292.
[24] D.R. Boston, J.C. Bailar, Inorg. Chem. 11 (1972) 1578–1583.
[25] D.C. Higgins, J.-Y. Choi, J. Wu, A. Lopez, Z. Chen, J. Mater. Chem. 22 (2012) 3727–3732.
[26] J. Choi, R. Hsu, Z. Chen, The Journal of Physical Chemistry C 114 (2010) 8048–8053.
[27] D. Lelievre, L. Bosio, J. Simon, J.J. Andre, F. Bensebaa, J. Am. Chem. Soc. 114 (1992) 4475–4479.
[28] N.B. McKeown, J. Mater. Chem. 10 (2000) 1979–1995.
[29] R. Bannehr, G. Meyer, D. Wöhrle, Polym. Bull. (Berlin) 2 (1980) 841–846.
[30] Z. Liu, X. Zhang, Y. Zhang, J. Jiang, Spectrochimica Acta Part A: Molecular and Biomolecular Spectroscopy 67 (2007) 1232–1246.
[31] P. Alessio, M.L. Rodriguez-Mendez, J.A. De Saja Saez, C.J.L. Constantino, Phys. Chem. Chem. Phys. 12 (2010) 3972–3983.
[32] R. Aroca, A. Thedchanamoorthy, Chem. Mater. 7 (1995) 69–74.
[33] L. Gaffo, C.J.L. Constantino, W.C. Moreira, R.F. Aroca, O.N. Oliveira, J. Raman Spectrosc. 33 (2002) 833–837.
[34] G. Faubert, G. Lalande, R. Côté, D. Guay, J.P. Dodelet, L.T. Weng, P. Bertrand, G. Dénès, Electrochim. Acta 41 (1996) 1689–1701.
[35] V. Nallathambi, J.-W. Lee, S.P. Kumaraguru, G. Wu, B.N. Popov, J. Power Sources 183 (2008) 34–42.
[36] F. Jaouen, F. Charreteur, J.P. Dodelet, J. Electrochem. Soc. 153 (2006) A689–A698.
[37] M. Lefèvre, J.P. Dodelet, Electrochim. Acta 48 (2003) 2749–2760.
[38] M. Lefèvre, J.P. Dodelet, Electrochim. Acta 53 (2008) 8269–8276.
[39] G. Liu, X. Li, P. Ganesan, B.N. Popov, Electrochim. Acta 55 (2010) 2853–2858.
[40] E.B. Easton, A. Bonakdarpour, J.R. Dahn, Electrochem. Solid-State Lett. 9 (2006) A463–A467.
[41] D. Higgins, Z. Chen, Z. Chen, Electrochim. Acta 56 (2011) 1570–1575.
[42] D.C. Higgins, J. Wu, W. Li, Z. Chen, Electrochim. Acta 59 (2012) 8–13.
[43] Z. Chen, D. Higgins, Z. Chen, Carbon 48 (2010) 3057–3065.
[44] R. Liu, D. Wu, X. Feng, K. Müllen, Angew. Chem. 122 (2010) 2619–2623.
[45] X. Li, H. Wang, J.T. Robinson, H. Sanchez, G. Diankov, H. Dai, J. Am. Chem. Soc. 131 (2009) 15939–15944.
[46] R. Seoudi, G.S. El-Bahy, Z.A. El Sayed, J. Mol. Struct. 753 (2005) 119–126.
[47] W. Lu, B. Zhao, N. Li, Y. Yao, W. Chen, Reactive and Functional Polymers 70 (2010) 135–141.
[48] K. Jia, R. Zhao, J. Zhong, X. Liu, J. Mater. Sci.: Mater. Electron. 21 (2010) 708–712.
[49] E. Charon, J.N. Rouzaud, J. Aléon, Carbon 66 (2014) 178–190.
[50] M. Sevilla, C. Sanchis, T. Valdes-Soli, E. Morallon, A.B. Fuertesta, Carbon 46 (2008) 931–939.
[51] G. Keru, P. Ndungu, V.O. Nyamori, J. Nanomat. 2013 (2013) 1–7.